Cluster size and composition variations in yellow and red light-emitting InGaN thin films upon thermal annealing

Shih-Wei Feng, Tsung-Yi Tang, Yen-Cheng Lu, Shi-Jiun Liu, En-Chiang Lin, C. C. Yang, Kung-Jen Ma, Ching-Hsing Shen, L. C. Chen, K. H. Kim, J. Y. Lin, and H. X. Jiang

Re-register for Table of Content Alerts

Create a profile.   Sign up today!

Cluster size and composition variations in yellow and red light-emitting InGaN thin films upon thermal annealing

Shih-Wei Feng,[a)] Tsung-Yi Tang, Yen-Cheng Lu, Shi-Jiun Liu, En-Chiang Lin, and C. C. Yang[b)]
Graduate Institute of Electro-Optical Engineering, Department of Electrical Engineering and Graduate Institute of Electronics Engineering, National Taiwan University, 1, Roosevelt Road, Sec. 4, Taipei, Taiwan, Republic of China

Kung-Jen Ma
Department of Mechanical Engineering, Chung Hua University, Hsinchu, Taiwan, Republic of China

Ching-Hsing Shen and L. C. Chen
Center for Condensed Matter Sciences, National Taiwan University, Taipei, Taiwan, Republic of China

K. H. Kim, J. Y. Lin, and H. X. Jiang
Department of Physics, Kansas State University, Manhattan, Kansas 66506-2601

We study thermal annealing effects on the size and composition variations of indium-aggregated clusters in two InGaN thin films with photoluminescence (PL) in the yellow and red ranges. The methods of investigation include optical measurement, nanoscale material analysis, and theoretical calculation. Such a study is important for determining the relation between the band gap and the average indium content of InGaN. In one of the samples, the major part of the PL spectrum is shifted from the yellow band into the blue range upon thermal annealing. In the other sample, after thermal annealing, a broad spectrum covering the whole visible range is observed. Cathodo-luminescence (CL) spectra show that the spectral changes occur essentially in the photons emitted from the shallow layers of the InGaN films. Photon emission spectra from the deeper layers are essentially unaffected by thermal annealing. The spectral changes upon thermal annealing are mainly attributed to the general trend of cluster size reduction. This interpretation is supported by the CL, x-ray diffraction, and high-resolution transmission electron microscopy results. To obtain a basic physics picture behind the spectral blue shift upon thermal annealing in the yellow emission sample, we theoretically study the quantum-confinement effects of InGaN clusters based on a quantum box model. The theoretical results can generally explain the large blue shift of PL spectral peak position. © *2004 American Institute of Physics.* [DOI: 10.1063/1.1703828]

I. INTRODUCTION

Recently, the characteristics of InN have become the subject of much attention. In particular, experimental data have shown that the band gap of InN is around 0.75 eV,[1,2] instead of the previously reported value 1.9 eV.[3] Such a dramatic change of InN band gap implies the need for careful examination of InGaN characteristics, particularly when the indium content is high. Also, the recently identified smaller band gap of InN implies that InGaN has the potential for an optoelectronics application in a much broader spectral range. With the average indium contents of lower than 30%, InGaN compounds have been widely used for the fabrications of UV, blue, and green light-emitting devices. However, studies on the optical properties and nanostructures in such compounds of relatively higher indium contents (emitting yellow, red, or even longer-wavelength photons) were rarely reported.[1,4] Recently, indium aggregation in InGaN has been

observed (see the discussions below). Such behavior implies that the reported InGaN band gaps may originate from indium-rich clusters, and are due to quantum confinement. They cannot be used for describing the bulk material properties of InGaN. The study on the indium aggregation phenomena, particularly when the average indium content is higher than 30%, can help us understand the relation between the InGaN band gap and its average indium content.

Due to the large lattice mismatch (11% in the *c* axis) between InN and GaN, their miscibility is quite low. In this situation, indium aggregation and phase separation can occur in InGaN through the process of spinodal decomposition.[5] In this process, the "up-hill" diffusion of indium atoms leads to the formation of high-indium InGaN clusters such that the strain energy can be released. Under certain conditions, the sizes of the clusters can be reduced to a few nanometers and strong quantum confinement is generated. In other words, InGaN quantum dots (QDs) can be formed. With such cluster structures, carriers can be localized in the potential minima for effective radiative recombination.[6–8] It is believed that the carrier localization mechanism is the key to the efficient photon emission in such a compound of high defect density

---
[a)]Current address: Department of Applied Physics, National University of Kaohsiung, No. 700, Kaohsiung University Rd., Nan-Tzu Dist., 811, Kaohsiung, Taiwan, Republic of China.
[b)]Electronic mail: ccy@cc.ee.ntu.edu.tw

($\sim 10^8$ cm^{-3}). Typically, the process of indium aggregation and hence the effect of carrier localization become stronger with increasing average indium content.[5,9] The effect of carrier localization has been regarded as one of the major mechanisms for the temperature-dependent S-shape variation of the photoluminescence (PL) spectral peak.[2,10] The temperature-dependent behavior originates from the localization of thermalized carriers and hence a blue shift of PL spectral peak in a certain temperature range. On the other hand, such an S-shape variation was also interpreted as the result of quantum-confined Stark effect (QCSE) in an InGaN/GaN quantum well (QW) structure.[11,12] QCSE originates from the strain-induced piezoelectric field distribution in a QW. The tilted potential leads to a red shift of the effective band gap. The existence of phonons at a relatively higher temperature can reduce the QCSE and generate a blue-shift trend.[13,14] The combination of the basic red shift (phonon effect) and the blue shift results in the S-shape behavior.

Post-growth thermal annealing can provide thermal energy for atomic rearrangement such that a thermal equilibrium state can be reached. It has been reported that post-growth thermal annealing could alter the sizes and distributions of self-organized InAs QDs.[15,16] In our previous studies, it was found that post-growth thermal annealing was quite effective for changing the cluster structures and their photon emission properties in InGaN/GaN QW samples.[17–19] This group has reported the formation of quasiregular quantum-dot-like structures from randomly distributed indium-aggregated clusters upon thermal annealing of an InGaN/GaN QW sample.[17] The effects of thermal annealing in QW samples of different well widths have also been studied.[18,19] It was discovered that under appropriate thermal annealing conditions, well-shaped QDs could be formed through spinodal decomposition in a narrow QW sample (well width $<$3 nm), leading to radiative efficiency improvement. However, in a sample of a relatively larger QW width (well width $>$3 nm), QD formation or optical quality improvement was not observed.[19]

Although indium aggregations through spinodal decomposition have been observed in InGaN/GaN QWs and thin films, their optical characteristics and nanostructures, particularly when the average indium content is higher than 30%, have not been well studied yet. Also, in such a sample, the effects of post-growth thermal annealing, which may further induce spinodal decomposition such that the equilibrium condition can be reached, have never been reported. In this article, we report the optical characteristics of two InGaN films with PL in the yellow and red ranges. In particular, the post-growth thermal annealing effects are discussed. In one of the samples, after thermal annealing, the PL spectral peak shifts from the yellow band into the blue range. This shift is particularly clear for photons emitted from the shallow portion of the InGaN thin film. In the other sample of even higher average indium content (red emission), the PL spectrum broadens to cover almost the whole visible range upon thermal annealing. The spectral changes are mainly attributed to the general trend of cluster shrinkage through spinodal decomposition. In the process of spinodal decomposi-

tion, the increase of indium composition within a cluster and the shrinkage of the cluster size may produce the counteraction between the red-shift and blue-shift trends. To determine the dominating mechanism, we use a simple but reasonable InGaN quantum cube model and theoretically study the quantum-confinement effects in nanometer-scale InGaN cluster. The theoretically predicted trend of PL peak position can generally explain the large blue-shift trend in PL peak position upon the thermal annealing process.

This paper is organized as follows: In Sec. II, sample structures and experimental procedures are described. In Sec. III, optical characterization results, including PL, photoluminescence excitation (PLE), and cathodo-luminescence (CL), are reported. Also, the x-ray diffraction (XRD) patterns are presented. In Sec. IV, theoretical results of band structure calculations are discussed. Finally, discussions and conclusions are given in Sec. V.

II. SAMPLE PREPARATION AND EXPERIMENTAL PROCEDURES

The two samples (designated as samples Y and R) used in this study were grown in a low-pressure metal-organic chemical vapor deposition reactor. In each sample, a $\sim$1.5 μm GaN epi-layer was deposited on a c-plane sapphire substrate with a 25 nm GaN buffer layer. The GaN epi-layer growth was followed by the deposition of a slightly silicon-doped InGaN film with a thickness of $\sim$0.15 μm. The average indium contents were estimated slightly higher than 30% and 40% in samples Y and R, respectively, determined by the indium and gallium flow rates during crystal growth. The silicon doping concentration was 4×10^{17} cm^{-3}. The growth temperatures of the GaN buffer layer, GaN epi-layer, and InGaN layer were 550, 1050, and 710 °C, respectively. In growing the GaN epi-layers and InGaN thin films, pressure of 325 torr was used. Trimethylgallium (TMGa) and trimethylindium (TMIn) were used as the precursors. The carrier gases for growing InGaN and GaN were nitrogen and hydrogen, respectively. High purity ammonia was used as the active nitrogen source. The GaN and InGaN growth rates were 3.6 and 0.3 μm/hr, respectively. Post-growth thermal annealing was conducted at 800 °C for 30 min in ambient nitrogen.

PL measurements were carried out with the 325 nm line of a 35 mW He–Cd laser for excitation. PLE experiments were performed using a quasimonochromatic excitation light source from a xenon lamp dispersed with a monochromator. The PLE detection photon energy was set at the PL spectral peak. The CL images were acquired using a Gatan monoCL3 spectrometer in a JEOL JSM 6700F SEM system. The kinetic energies of electrons for CL measurements ranged from 3 to 15 keV with an electron beam current of 60–300 pA. The surface spatial resolution is about 100 nm. In addition, XRD measurements were carried out using Cu K radiation, monochromated with the (111) reflection of Ge single crystal. The high-resolution transmission electron microscopy (HRTEM) investigations were performed using a Philips TECNAI F20 field-emission electron microscope with an accelerating voltage of 200 kV. All high-resolution micrographs were taken at the Scherzer defocus. The samples were viewed along a [11–20] zone axis for bright-field images. To
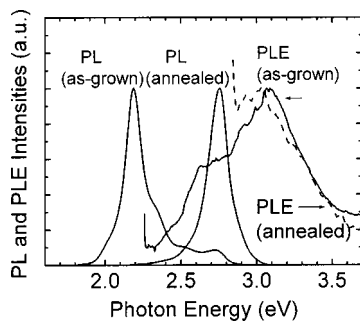
FIG. 1. PL and PLE spectra at 10 K before and after thermal annealing of sample Y.

FIG. 2. PL and PLE spectra at 10 K before and after thermal annealing of sample R.

clearly show the compositional variations in InGaN alloy, digital micrograph 3.7.4 software was utilized to sharpen the boundaries between indium-rich clusters and the surrounding compounds.

III. CHARACTERIZATION RESULTS

Figure 1 shows the PL and PLE spectra at 10 K of the as-grown and annealed samples Y. It is noted that PL spectral peak of this sample has shifted from the yellow band (around 2.2 eV) to the blue range (around 2.75 eV) after thermal annealing. The blue-emission contribution as a small side-lobe can also be observed in the PL spectrum of the as-grown sample. Usually, PL emission essentially originates from a shallow layer of the sample. Therefore, we can exclude the possibility that the yellow-band emission comes from the defects in GaN.[20] The PLE spectrum of the as-grown sample Y shows multiple InGaN absorption peaks, corresponding to the clusters of different geometries and compositions. The Stokes shift (SS) of the PL peak with respect to the PLE absorption maximum (around 3.05 eV) is as large as about 1 eV, indicating the strong indium composition fluctuation and/or strong QCSE. After thermal annealing, the spectral position of the major absorption peak near 3.05 eV is unchanged. This energy level may correspond to the background indium composition, on top of which higher indium compositions fluctuate, in the as-grown and annealed samples. The distribution of the higher indium composition fluctuation varied upon thermal annealing such that the PL spectrum blue-shifted and the SS became quite small (around 200 meV). However, it seems that the background indium composition did not change upon thermal annealing.

Figure 2 shows the PL spectra of the as-grown and annealed samples R and the PLE spectrum of the as-grown sample R at 10 K. After thermal annealing, the luminescence shows multiple-band emission including red, green, and blue, which may come from the contributions of InGaN clusters of different compositions and sizes. In other words, upon thermal annealing the nanostructures of part of the clusters were changed to emit shorter-wavelength photons. The large SS (1.1 eV) of the as-grown sample R shows the stronger indium composition fluctuation and/or QCSE when compared with the as-grown sample Y. It is noted that after thermal annealing, photon emission from sample R became quite
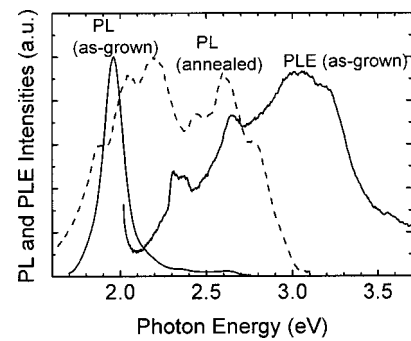
dim such that the measurement of its PLE spectrum was difficult.

Figure 3 shows the typical CL images of the as-grown (a) and annealed (b) samples Y, both with the excitation of 3 kV electrons. The 3 kV represents the electron acceleration voltage and roughly corresponds to a penetration depth of 88 nm. Therefore, only the shallow portions of the InGaN thin films are excited. The light spots of a few hundred nanometers in size in the CL image of the as-grown sample Y emit essentially yellow and relatively weaker blue photons. They are supposed to correspond to the indium-aggregated clusters. After thermal annealing, the CL image becomes blurred. Actually, the image in Fig. 3(b) consists of many tiny light spots at the order of 100 nm in size, which is close to the spatial resolution of the used CL system. Those tiny light spots essentially emit blue light. The generation of those tiny light spots implies that the cluster sizes in the InGaN film might be generally reduced upon thermal annealing, particularly in the shallow portion. Figure 4 shows the typical CL images of the as-grown (a) and annealed (b) samples Y, both
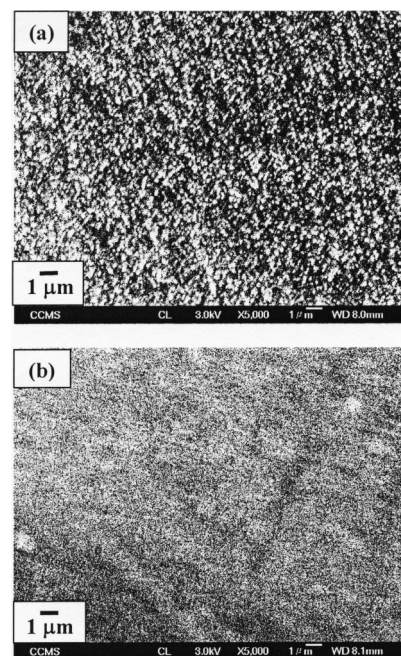
FIG. 3. Typical CL images before (a) and after (b) thermal annealing of sample Y with the excitation of 3 kV electron voltage.
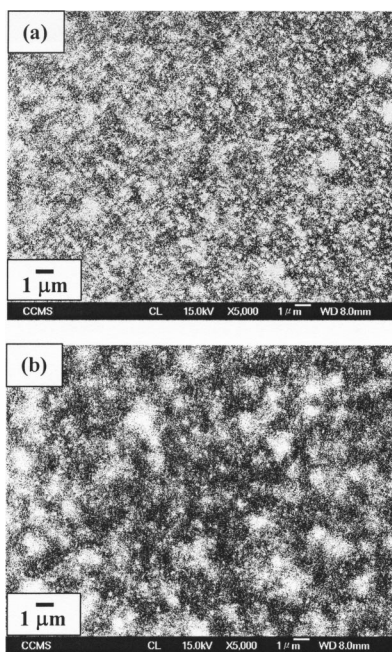
FIG. 4. Typical CL images before (a) and after (b) thermal annealing of sample Y with the excitation of 15 kV electron voltage.

FIG. 5. Typical CL images before (a) and after (b) thermal annealing of sample R with the excitation of 3 kV electron voltage.

with the excitation of 15 kV electrons. The 15 kV accelerating voltage roughly corresponds to the penetration depth of 1300 nm, deep into the GaN layer beneath. The comparison between Figs. 4(a) and 4(b) shows the same trend of tiny light spot generation upon thermal annealing as the case of 3 kV-electron excitation. Also, compared with the 3 kV CL image [see Fig. 3(a)], the sizes of individual bright spots in the 15 kV image are smaller. However, large bright areas (in the dimension of micrometers), consisting of many smaller spots, are formed. They are observed because a CL image is obtained by accumulating the luminescence along the depth. The same argument can be applied to the annealed sample Y.

Figure 5 shows the typical CL images of the as-grown (a) and annealed (b) samples R, both with the excitation of 3 kV electrons. Compared with the CL image of the as-grown sample Y [see Fig. 3(a)], that of the as-grown sample R shows light spots of a larger variety in size. This observation is consistent with the speculation of the stronger indium composition fluctuation in the as-grown sample R based on the PLE results. After thermal annealing of sample R, the CL image seems almost featureless. Nearly uniform tiny light spots, with the sizes close to the spatial resolution of the CL system, are observed. Such an observation also implies the general trend of cluster shrinkage upon thermal annealing.

Figures 6(a) and 6(b) show the CL spectra of the as-grown and annealed samples Y, respectively. In each sample, the 3, 5, 8, and 15 kV electron voltages roughly correspond to the penetration depths of 88, 210, 450, and 1300 nm, respectively. In the as-grown sample, luminescence mainly in the yellow band is observed in a shallow layer (3 kV probe). With increasing electron voltage, not only the yellow band, but also the peak of blue luminescence (between 2.7 and 2.85 eV) can be observed. Also, with 8 and 15 kV electron excitations, the luminescence from the GaN layer
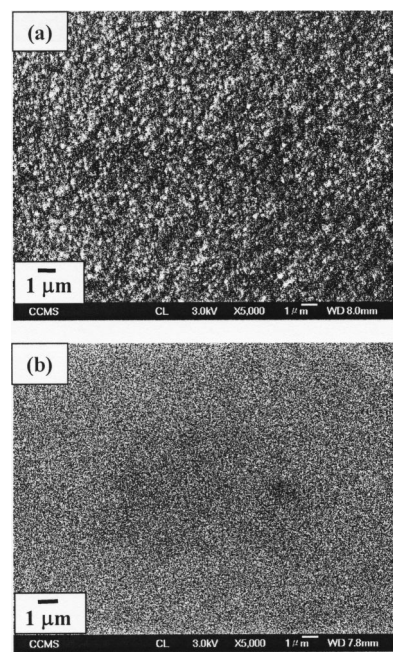
(around 3.4 eV) can be clearly seen. Hence, it is believed that certain nanostructures, existing in the deep portion of the InGaN film, can emit photons in the blue range. This result is consistent with the side-lobe of the PL spectrum in the as-grown sample, as shown in Fig. 1. After thermal annealing, in the shallow layer of the InGaN film (3 kV probe), only blue luminescence exists, that is again consistent with the PL measurement. With excitation of higher-energy electrons, the blue luminescence is enhanced and the GaN emission peak appears. Also, a broad yellow luminescence band is observed. This yellow luminescence is believed to originate from the defects in the GaN layer, instead of the cluster luminescence in the InGaN film. From the results described above, we speculate that after thermal annealing, the nanostructure of the shallow layer of the InGaN film has been changed into that similar to the structure resulting in blue
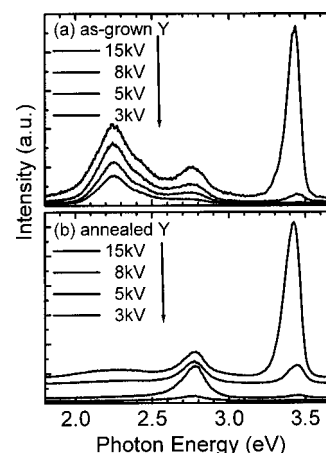
FIG. 6. CL spectra with the excitations of 3, 5, 8, and 15 kV electron voltages for the as-grown (a) and annealed (b) samples Y. All measurements were performed at room temperature.
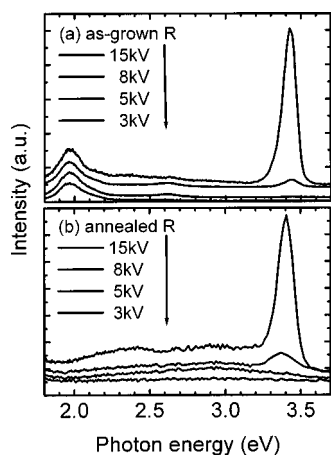
FIG. 7. CL spectra with the excitations of 3, 5, 8, and 15 kV electron voltages for the as-grown (a) and annealed (b) samples R. All measurements were performed at room temperature.

FIG. 8. XRD patterns of the as-grown samples Y and R.

luminescence in the deeper portion. Hence, the whole InGaN film emits blue light. The different nanostructures between the shallow and deep portions in the as-grown InGaN film can be due to the fact that in growing the shallow portion, the high growth temperature had an effect of thermally annealing the deep portion. The other possible reason for the different nanostructures between the shallow and deep layers is the effect of composition pulling in growing InGaN films.[21,22] In other words, the average indium content in the shallow layer is higher than that in the deep layer. Different average indium contents result in different aggregation structures and hence different photon emission spectra. In our study, it is found that the deep-layer nanostructure does not seem to vary much upon thermal annealing. However, that in the shallow layer changes significantly.

Figures 7(a) and 7(b) show the CL spectra of the as-grown and annealed samples R, respectively, with different electron acceleration voltages. In the as-grown sample, only red luminescence is observed in a shallow layer (3 kV probe). With higher excitation voltages, not only the red band but also the broad visible range, particularly a small peak of blue luminescence (between 2.5 and 2.7 eV), can be observed. With increasing electron voltage, eventually the luminescence of the GaN layer appears. Hence, different nanostructures exist at different depths of the InGaN film in the as-grown sample R, leading to a broad spectrum of photon emission. This result is also consistent with the long tail on the high-energy side of the PL spectrum in the as-grown sample, as shown in Fig. 2. After thermal annealing, broad CL spectra over the ranges of the visible and UV can always be observed with various excitation electron voltages [see Fig. 7(b)], that is again consistent with the PL spectrum, as shown in Fig. 2. Such results confirm the hypothesis of randomly distributed cluster structures of different sizes and compositions in the annealed sample R.

Figure 8 shows the XRD patterns of the as-grown samples Y and R. Besides the GaN peak (C), the nearly pure InN peak (A), and the InGaN distribution (B), corresponding to indium composition fluctuation, clearly indicate strong indium aggregation processes in the samples. In these two and
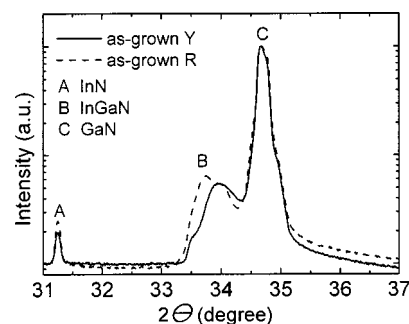
all other InGaN samples previously studied by this group, the distribution B always terminates at around $2\theta=33.2°$, implying the solubility limit of InN in GaN at around 41%. This solubility limit is obtained based on a simple calculation of linear interpolation. It is noted that InGaN within a cluster is under compressive strain (affected by the surrounding InGaN of a lower indium composition). In other words, the calibrated indium composition based on the XRD measurement could be underestimated.

In the comparison between the as-grown samples Y and R, the broader distribution B and higher peak A in sample R once again confirm its stronger indium composition fluctuation. We have also compared the XRD patterns between the as-grown and annealed samples Y.[23] After thermal annealing of the sample, the distribution B splits into two components. The low-indium component is attached to the GaN peak. This phenomenon may imply a larger contrast of indium concentration between a cluster and the surrounding region. The component attaching to the GaN peak is related to the composition of the region surrounding the formed clusters.

The InGaN cluster formation and InN solubility limit in GaN have important implications in the related studies. Recently, because of the interest in InN characteristics, the relation between material band gap and indium composition has been studied.[1,2] In such a study, caution needs to be taken in the measurement of material band gap. Because of the clustering nature of InGaN, the emitted photons for band gap determination mainly come from clusters, which may bear the quantum-confinement effect. In this situation, the calibrated energies are actually not the bulk material band gaps. Also, with the aforementioned solubility limit, the nanostructures of InGaN compounds of high average indium contents need to be carefully analyzed before one can determine their correct material band gaps.

Figures 9(a) and 9(b) show the HRTEM images of the as-gown and annealed samples Y, respectively. The arrows show the directions of crystal growth. The cluster domain structures in both samples can be clearly seen. Although the domain geometry in either sample is quite random, one still can observe that the domain size in the annealed sample Y is generally smaller than that of the as-grown sample. During thermal annealing, spinodal decomposition generally reduces the cluster sizes in the case of our study. In this process, the indium content in an InGaN cluster is expected to increase. The increase of indium content is supposed to reduce the effective band gap. However, the shrinkage of cluster size

J. Appl. Phys., Vol. 95, No. 10, 15 May 2004

Feng *et al.* 5393
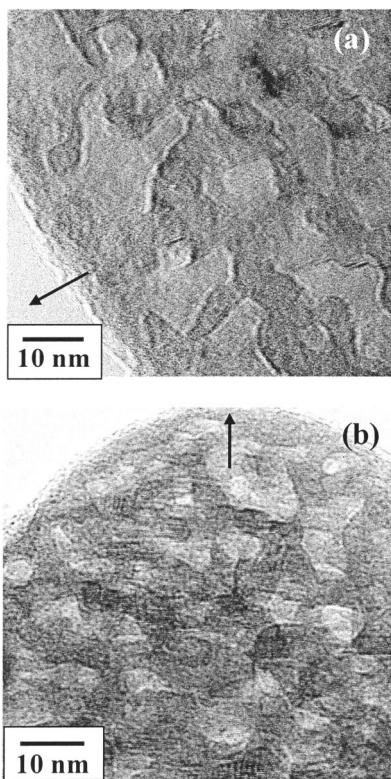
FIG. 9. HRTEM images of the as-grown (a) and annealed (b) samples Y. The arrows show the crystal growth directions.

FIG. 10. Schematic drawing of the band structure of a quantum cube with size L.

should result in stronger quantum confinement and increase the effective band gap. The counteraction between the two mechanisms actually led to the significant blue shift in the PL spectrum of sample Y. In the next section, we will use a quantum cube model to calculate the effective band gap of a cluster with the experimental conditions taken into consideration. The aforementioned counteraction will be examined.

IV. THEORETICAL STUDY

To understand the blue-shift behaviors of the PL spectral peak upon thermal annealing, we performed a theoretical study by calculating the ground-state levels of a quantum box based on a series-expansion model. In the calculations, we used certain experimental data of sample Y as input parameters, including PL spectral peaks for the energy levels of the effective band gaps, PLE spectra and XRD patterns for the estimates of indium compositions, and HRTEM images for the sizes of indium-aggregated clusters.

In our calculations, the theory of a series expansion based on the eigen-functions of infinity barrier for the discrete-state wave functions is used.[24,25] The strain effect is included by evaluating the lattice mismatch between the indium compositions of a cluster and the surrounding compound. For simplicity, we neglect the effect of electron-hole Coulomb interaction. In other words, the exciton effect is ignored. Although the exciton binding energy of GaN is quite large ($\sim$30 meV), those of the InGaN compounds with high indium compositions in our samples are still unknown. The exciton binding energy usually decreases with decreasing band gap. Although strong quantum confinement can en-

hance the exciton binding energy, it has been pointed out that the increase of effective band gap in energy discretization is more important than the enhancement of exciton binding energy in calculating the effective band gap of a QD.[15] Therefore, in our model, it is reasonable to ignore the exciton effect.

With the exciton effect ignored, the equations for the electron and hole wave functions can be decoupled. The wave function solutions of electron and hole can be expressed as the series expansions of the complete sets of ortho-normal eigen-functions, with properly chosen coefficients, of a quantum box with the assumption that the barrier potential is infinitely high. With the barrier of infinite height, the amplitudes of the eigen-functions decay to zero at the box boundaries. However, with the finite barrier height in the real situation, wave functions extend into the barrier to a certain distance. To include the wave function penetration into the barrier, we choose the dimensions of the infinity-barrier quantum box to be twice those of the real quantum box, following an empirical conclusion.[25] This choice of the empirical factor can slightly influence the numerical results. However, the key physics is unaffected. After certain derivations, we can obtain a matrix eigen-problem, which is to be solved numerically. Ten terms are considered in the aforementioned series expansion for each dimension.

In general, with compressive strain in the quantum-confined region, the conduction-band and valence-band edges are shifted upward and downward, respectively. The strain-induced band structure modification of a quantum dot can be expressed with a product of strain components by a deformation potential.[15] With hydrostatic strains, the strain effects of the conduction band are decoupled from those of the valence band. In the following, we assume that strain is zero outside the quantum box and is compressive inside, as depicted in Fig. 10. In this situation, at the Γ point, the conduction- and valence-band edges are modified by the energy shifts δE_c and δE_v, respectively.[15] In Fig. 10, E_n^c (E_n^v) ($n=0,1,2,...,$) represent the discrete energy levels in the conduction (valence) band. They are to be obtained by numerically solving the aforementioned matrix eigen-problem. Also, E_g is the material band gap of the InGaN compound inside the quantum box.

Table I lists the physical parameters used in our calculations. We use an edition of the band-gap energy for $In_xGa_{1-x}N$ as given in Ref. 1. The band-edge discontinuity

TABLE I. Material parameters of GaN and InN used for calculations.

	GaN	InN
Lattice constant (Å)[a]		
a	3.189	3.545
c	5.185	5.703
Effective mass[b] $m=(m_\parallel m_\perp^2)^{1/3}$		
Electron mass along the c-axis $m_\parallel$	$0.19\,m_0$	$0.11\,m_0$
perpendicular to the c-axis $m_\perp$	$0.17\,m_0$	$0.1\,m_0$
	$1.76\,m_0$	$1.56\,m_0$
Heavy hole mass along the c-axis $m_\parallel$	$1.69\,m_0$	$1.68\,m_0$
perpendicular to the c-axis $m_\perp$		
(m_0: free electron mass)		
Hydrostatic deformation potential (eV)[a]		
Conduction-band a_c	6	3
Valence-band a_v	0.8	0.5

[a]Reference 26.
[b]Reference 27.

(band offset) ratio for the conduction and valence bands is assumed to be 0.67:0.33.[27] We calculate the parameters of $In_xGa_{1-x}N$, other than material band gap energy, with the linear interpolation formula.

In our numerical calculations, we consider a quantum cube with the dimension L. Also, the indium composition of the barrier is fixed at 8%. This percentage is determined with the major absorption peak of the PLE spectra (around 3.05 eV) of the as-grown and annealed samples Y, as shown in Fig. 1. With $E_g(x)=3.05$ eV, we can obtain $x=0.08$. This composition is consistent with the attached side-lobe (around $2\theta=34.4°$) of the GaN peak in the XRD pattern of the annealed sample Y.[23]

Figure 11 shows E_0^c values as functions of indium composition for several quantum cube sizes. With the same cube size, the E_0^c value increases with the indium composition inside the cube. As indium composition increases, the smaller electron effective mass of InGaN results in the increasing trend of E_0^c although the material band gap decreases. In addition, with the same composition inside the quantum cube, the variation of E_0^c is more sensitive to the change of cube size as indium composition increases. The smaller electron effective mass of InGaN with a higher indium composition can also explain this trend. It is noted that a bound state may not exist in the quantum cube if the composition contrast or the cube size is too small.[13] Figure 12 shows the E_0^v values as functions of cube indium composition for several cube sizes. Their general trends are the same
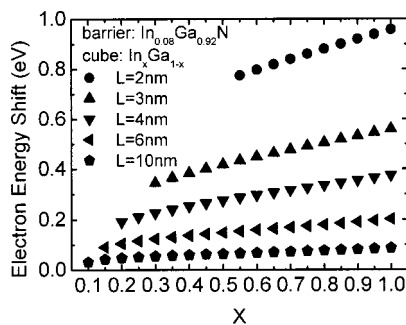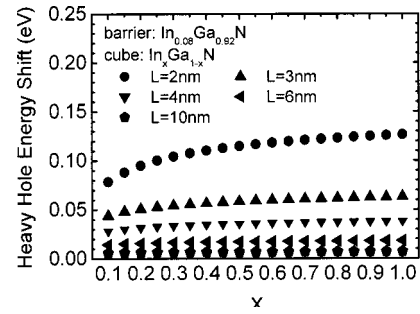
FIG. 12. Heavy hole energy shifts (E_0^v) as functions of the indium composition in the quantum cube for several quantum cube sizes.

as those of the electron. Figure 13 shows hydrostatic-strain-induced energy shifts δE_c and δE_v as functions of the indium composition in the cube for the conduction and valence bands. As indium composition increases, the lattice mismatch between the cube and barrier becomes larger and hence the strain effect is enhanced.

With the calculation results based on the quantum cube model, we are ready to compare the theoretical predictions with the experimental data. As shown in Fig. 14, we plot the electron transition energies, corresponding to the transition between the ground electron state and the ground heavy-hole state, versus the indium composition in the cube for several cube sizes. These transition energies, denoted by E_{PL}, is defined as

$$E_{PL}\equiv E_0^c+\delta E_c+E_g+\delta E_v+E_0^V. \qquad (1)$$

At low temperatures, optically excited electrons and holes relax to individual ground states before recombination. Therefore, we can assume that the measured PL spectral peak corresponds to the energy E_{PL}. In Fig. 14, the dashed curve represents the material band gap of $In_xGa_{1-x}N$ inside the cube. With the same cube size, the difference between E_{PL} and the material band gap becomes larger as indium composition increases. Comparing with the experimental data, we plot two horizontal lines in Fig. 14 to indicate the PL spectral peaks of the as-grown and annealed samples Y. From the HRTEM images, one can assume 10 nm for the indium-aggregated cluster size in the as-grown sample Y and 2–4 nm in the annealed sample Y. The assumptions lead to the conclusion that the indium compositions in the cube are around 45% before annealing and around 55% after annealing, with the two points connected by the arrow in Fig. 14.

FIG. 11. Electron energy shifts (E_0^c) as functions of the indium composition in the quantum cube for several quantum cube sizes.
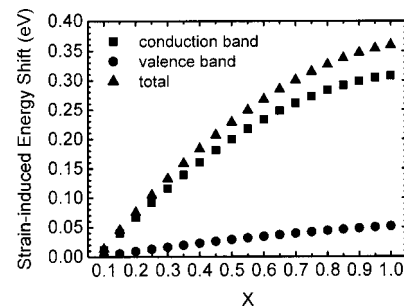
FIG. 13. Hydrostatic strain-induced energy shifts δE_c and δE_v as functions of the indium composition in the quantum cube.
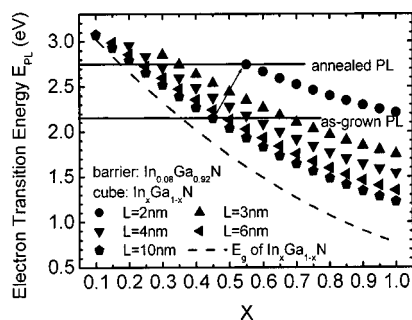
FIG. 14. Electron transition energies (E_{PL}) as functions of the indium composition in the quantum cube for several quantum cube sizes.

The results of 45% indium composition before annealing and 55% composition after annealing seem to contradict the solubility limit calibrated from the XRD measurements. Several possible explanations are given as follows: (1) as discussed in Sec. III, the solubility of 41% indium from XRD measurements is underestimated; (2) it is noted that in the real situation, the cluster interfaces are not as sharp as those of the assumed quantum cube in the theoretical calculations. Hence, the strains built in the QDs are expected to be weaker than the theoretical predictions. Therefore, the data curves in Fig. 14 are lower than those as shown. In other words, the indium compositions in the samples before and after thermal annealing can be lower than those described above; and (3) from the optical measurements, such as PLE, the QCSE can be significantly released after thermal annealing. Hence, the blue shift after annealing may not be completely due to the shrinkage of clusters. Although it is uncertain, the quantum dot may not be as small as 2 nm in size. The effect of QCSE relaxation deserves further investigation.

V. DISCUSSIONS AND CONCLUSIONS

Because of the relatively higher thermal annealing temperature (800 °C), compared with the InGaN growth temperature (710 °C), desorption of InN from the InGaN layer could occur during thermal annealing. Such a process could reduce the indium content and shrink the cluster size in the shallow layer of a sample. However, we speculate that this process is a minor one because based on the theoretical results in the last section, the indium composition in a cluster needs to be increased such that the significant PL blue shift after thermal annealing in sample Y can be well explained.

In summary, we have studied the indium aggregation phenomena in two InGaN thin films with PL in the yellow and red ranges and their variations upon post-growth thermal annealing through optical measurements, material analyses, and theoretical calculations. The Stokes shifts of the PL spectral peaks with respect to the major PLE absorption peaks in the as-grown samples could be as large as 1 eV, indicating the strong indium composition fluctuations and/or strong QCSEs. In one of the samples, the major part of PL spectrum was shifted from the yellow band into the blue range upon thermal annealing. In the other sample, after thermal annealing, a broad spectrum covering the whole visible range was observed. CL spectra showed that the spectral changes occurred essentially in the photons emitted from the shallow layers of the InGaN films. Photon emission spectra from the deeper layers were essentially unaffected by thermal annealing. The spectral changes upon thermal annealing were mainly attributed to the general trend of cluster size reduction. The interpretation was supported by the CL, XRD, and HRTEM results. To obtain a basic physics picture behind the spectral blue shift upon thermal annealing in the yellow emission sample, we theoretically studied the quantum confinement effects of the InGaN clusters based on a quantum cube model. The theoretical results generally explained well the large blue shift in PL spectral peak position.

[1] J. Wu, W. Walukiewicz, K. M. Yu, J. W. Ager III, E. E. Haller, Hai Lu, and William J. Schaff, Appl. Phys. Lett. **80**, 4741 (2002).

[2] T. Matsuoka, H. Okamoto, M. Nakao, H. Harima, and E. Kurimoto, Appl. Phys. Lett. **81**, 1246 (2002).

[3] K. L. Westra, R. P. W. Lawson, and M. J. Brett, J. Vac. Sci. Technol. A **6**, 1730 (1988).

[4] F. B. Naranjo, M. A. Sánchez-García, F. Calle, E. Calleja, B. Jenichen, and K. H. Ploog, Appl. Phys. Lett. **80**, 231 (2002).

[5] Y. S. Lin, K. J. Ma, C. Hsu, S. W. Feng, Y. C. Cheng, C. C. Liao, C. C. Yang, C. C. Chou, C. M. Lee, and J. I. Chyi, Appl. Phys. Lett. **77**, 2988 (2000).

[6] Y. Narukawa, Y. Kawakami, S. Fujita, S. Fujita, and S. Nakamura, Phys. Rev. B **55**, R1938 (1997).

[7] S. F. Chichibu, K. Wada, J. Müllhäuser, O. Brandt, K. H. Ploog, T. Mizutani, A. Setoguchi, R. Nakai, M. Sugiyama, H. Nakanishi, K. Korii, T. Deguchi, T. Sota, and S. Nakamura, Appl. Phys. Lett. **76**, 1671 (2000).

[8] Y. Narukawa, Y. Kawakami, S. Fujita, and S. Nakamura, Phys. Rev. B **59**, 10 283 (1999).

[9] C. C. Liao, S. W. Feng, C. C. Yang, Y. S. Lin, K. J. Ma, C. C. Chuo, C. M. Lee, and J. I. Chyi, Appl. Phys. Lett. **76**, 318 (2000).

[10] Y. H. Cho, G. H. Gainer, A. J. Fischer, J. J. Song, S. Keller, U. K. Mishra, and S. P. DenBarrs, Appl. Phys. Lett. **73**, 1370 (1998).

[11] S. F. Chichibu, A. C. Abare, M. S. Minsky, S. Keller, S. B. Fleischer, J. E. Bowers, E. Hu, U. K. Mishra, L. A. Coldren, S. P. DenBaars, and T. Sota, Appl. Phys. Lett. **73**, 2006 (1998).

[12] E. Berkowicz, D. Gershoni, G. Bahir, E. Lakin, D. Shilo, E. Zolotoyabko, A. C. Abare, S. P. Denbaars, and L. A. Coldren, Phys. Rev. B **61**, 10 994 (2000).

[13] P. Perlin, Ch. Kisielowski, V. Iota, B. A. Weinstein, L. Mattos, N. A. Shapiro, J. Kruger, E. R. Weber, and J. Yang, Appl. Phys. Lett. **73**, 2778 (1998).

[14] P. Riblet, H. Hirayama, A. Kinoshita, A. Hirata, T. Sugano, and Y. Aoyagi, Appl. Phys. Lett. **75**, 2241 (1999).

[15] D. Bimberg, M. Grundmann, and N. N. Ledentsov, *Quantum Dot Heterostructures* (Wiely, England, 1999).

[16] T. M. Hsu, Y. S. Lan, W.-H. Chang, N. T. Yeh, and J.-I. Chyi, Appl. Phys. Lett. **76**, 691 (2000).

[17] Y. S. Lin, K. J. Ma, C. Hsu, Y. Y. Chung, C. W. Liu, S. W. Feng, Y. C. Cheng, M. H. Mao, C. C. Yang, H. W. Chuang, C. T. Kuo, J. S. Tsang, and T. E. Weirich, Appl. Phys. Lett. **80**, 2571 (2002).

[18] L. T. Romano, M. D. McCluskey, B. S. Krusor, D. P. Bour, C. Chua, S. Brennan, and K. M. Yu, J. Cryst. Growth **189/190**, 33 (1998).

[19] Y. Y. Chung, Y. S. Lin, S. W. Feng, Y. C. Cheng, E. C. Lin, C. C. Yang, K. J. Ma, C. Hsu, H. W. Chuang, C. T. Kuo, and J. S. Tsang, J. Appl. Phys. **93**, 9693 (2003).

[20] D. Vanderbilt and L. K. Wickham, Mater. Res. Soc. Symp. Proc. **202**, 555 (1991).

[21] S. Pereira, M. R. Correia, E. Pereira, K. P. O'Donnell, C. Trager-Cowan, F. Sweeney, and E. Alves, Phys. Rev. B **64**, 205 311 (2001).

[22] M. Hao, H. Ishikawa, T. Egawa, C. L. Shao, and T. Jimbo, Appl. Phys. Lett. **82**, 4702 (2003).

[23] S. W. Feng, E. C. Lin, T. Y. Tang, Y. C. Cheng, H. C. Wang, C. C. Yang, K. J. Ma, C. H. Shen, L. C. Chen, K. H. Kim, J. Y. Lin, and H. X. Jiang, Appl. Phys. Lett. **83**, 3906 (2003).

[24] H. Gotoh, H. Ando, T. Takagahara, H. Kamada, A. Chavez-Pirson, and J. Temmyo, Jpn. J. Appl. Phys., Part 1 **36**, 4202 (1997).

[25] S. Gangopadhyay and B. R. Nag, Nanotechnology **8**, 14 (1997).

[26] Y. C. Yeo, T. C. Chong, and M. F. Li, J. Appl. Phys. **83**, 1429 (1998).

[27] S. L. Chung, IEEE J. Sel. Top. Quantum Electron. **32**, 1791 (1996).